Analysis of trapping effects on the forward current-voltage characteristics of Al implanted 4H-SiC p-i-n diodes

M. L. Megherbi, F. Pezzimenti, L. Dehimi, A. Saadoune, and F. G. Della Corte, *Senior Member IEEE*

***Abstract*—The forward current-voltage characteristics (I_F-V_F) of aluminum (Al) implanted 4H-SiC p-i-n diodes are investigated by means of a numerical simulation study that takes into account both intrinsic and doping-induced deep-defects, namely the $Z_{1/2}$ and $EH_{6/7}$ centers inside the drift region and an electrically active trap concentration inside the anode region due to the Al^+ ion implantation process. From the experimental results, the fundamental electric parameters of several samples were extracted at different regions of diode operation and used for comparison. The modelling analysis reveals that $Z_{1/2}$ and $EH_{6/7}$ centers reduce the effective carrier lifetimes and increases the recombination rate in the drift region determining the slope of the I_F curve in the recombination and diffusion regimes. In addition, a defect density that becomes comparable to the epilayer doping concentration introduces an apparent shunt resistance effect at low-medium biases and at the same time has a noticeable impact on the diode series resistance at voltages higher than 2.7 V. A detrimental effect on the series resistance is also observed in dependence of the trap concentration in the anode region that increases the diode internal resistance as a consequence of the carrier mobility decrease. Above the I_F curve knee the diode current is largely dominated by the electron injection into the anode since the concentration of free holes for conduction is strongly limited in turn by the incomplete activation of the ion implanted impurities and the trap activity.**

***Index Terms*—4H-SiC, p-i-n diodes, device modeling, defect states, ideality factor, series resistance.**

I. Introduction

DURING the last decade, a large variety of silicon carbide (SiC) based devices have been extensively proposed for high-power, high-frequency, and high-temperature applications [1]-[4]. The 4H-SiC polytype, in particular, is a wide-bandgap semiconductor with excellent electronic properties that can withstand a breakdown electric field (2.5 MV/cm) over eight times greater than Si or GaAs [5]. Also, compared to these conventional materials, 4H-SiC exhibits a two time greater saturated carrier velocity, i.e. 2×10^7 cm/s, and a thermal conductivity in the order of 3.5-4 W/K×cm whereas typical values for Si and GaAs are 1.5 W/K×cm and 0.5 W/K×cm, respectively.

However, since the 4H-SiC is a relatively new technology, the deployment of intensive efforts, based in turn on numerical (or analytical) and experimental analyses, are needed to investigate the material physical parameters that affect the device electrical characteristics. Among the major 4H-SiC technological issues, we can certainly consider the presence of intrinsic deep defects in the starting substrates and epilayers, as well as the control of defect concentrations unavoidably introduced during the doping processes [6]-[8]. In fact, depending on their concentration and capture cross sections, defects act for carriers either as traps or as recombination centers [8]-[11]. Traps determine a reduction of the free carrier concentrations whereas recombination centers introduce generation-recombination currents in rectifying devices [11]-[13]. For these important scattering mechanisms, as far as we know, experimental or theoretical data are not commonly available yet.

This paper is therefore addressed to investigate the experimental forward current-voltage characteristics of aluminum (Al) implanted 4H-SiC p-i-n diodes with modeling of recombination and trapping effects due to both intrinsic and doping-induced deep-defects. More in detail, in order to gain control and understanding of defect activity, during the simulations an explicit concentration of $Z_{1/2}$ and $EH_{6/7}$ centers inside the epitaxial layer and an electrically active trap concentration due to the Al^+ ion implantation process of the anode region were taken into account by using a fine-tuned combined model. It allows to achieve a very good agreement with the experimental results in terms of ideality factor and series resistance at the different regions of diode operation in a current range that spans over ten decades. Preliminary results assuming the defect effects independent each other in determining the device current capabilities were previously presented in [14]. Moreover, in this work the attention is focused on the carrier injection and recombination depth profiles inside the p-i-n structure.

II. Device Structure

A schematic cross-section of the 4H-SiC p-i-n diodes considered in this work is shown in Fig. 1 (plot not in scale). Here, the Al implanted profile as a function of the distance from the anode contact is also reported. The diodes were

M.L. Megherbi and A. Achour are with Laboratory of Metallic and Semiconducting Materials, Mohammed Khieder University, 07000 Biskra, Algeria.

F. Pezzimenti and F.G. Della Corte are with Università Mediterranea di Reggio Calabria, DIIES, 89100 Reggio Calabria, Italy (e-mail: fortunato.pezzimenti@unirc.it).

L. Dehimi is with Faculty of Science, Elhadj Lakhdar University, 05000 Batna, Algeria.

provided by the CNR Institute for Microelectronics and Microsystems, Unit of Bologna - Italy. They are based on a <0001> 8° off-axis n/n$^+$ 4H-SiC epitaxial wafer and perform a theoretical breakdown voltage of 1 kV. The epilayer thickness is 5 μm and the epilayer doping is 3×10^{15} cm^{-3}. During the fabrication, the anode region was realized by multiple implantation doses of Al at 673 K on selected circular areas with a diameter in the range 150-1000 μm [15]. The anode and cathode ohmic contacts were made by deposition of titanium-aluminum (Ti/Al) dots on the p$^+$ implanted regions and a nickel (Ni) film on the n$^+$ back surface of the wafer, respectively. The measured anode contact resistance is in the order of 1.5 mΩ×cm^2 at room temperature [15]. This value is typical for Ti/Al depositions on *p*-type 4H-SiC substrates with doping concentrations in excess of 2×10^{19} cm^{-3} [16].

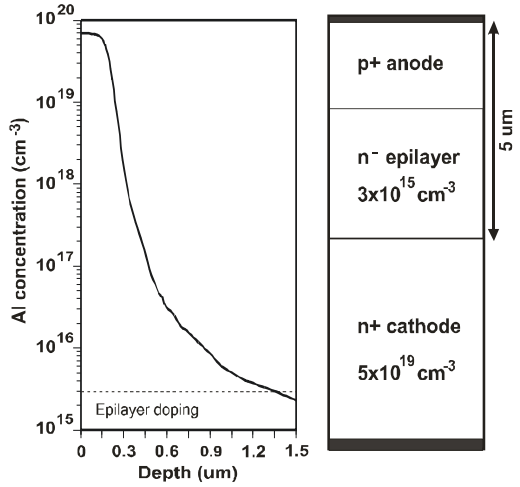

Fig. 1. 4H-SiC p-i-n diode schematic cross section and Al implanted profile along the device.

The implanted profile assures an Al concentration of 6×10^{19} cm^{-3} up to 0.2 μm from the diode surface and then it decreases with an half-Gaussian shape crossing the epilayer doping at 1.35 μm as verified by secondary ion mass spectroscopy (SIMS) measurements [17], [18].

III. Simulation Setup

The simulation analysis was carried out using a TCAD 2D physical simulator [19] by solving the Poisson's equation and the carrier continuity equations:

$$\varepsilon\nabla^2\psi = -q(p - n + N_D^+ - N_A^-) - Q_t \tag{1}$$

$$\frac{\partial n}{\partial t} = \frac{1}{q}\nabla J_n - U_n \tag{2}$$

$$\frac{\partial p}{\partial t} = \frac{1}{q}\nabla J_p - U_p . \tag{3}$$

Here, ψ is the intrinsic Fermi potential, ε is the electrical permittivity, q is the electronic charge, n and p are the electron and hole concentrations, Q_t is the charge due to traps and defects, N_D^+ and N_A^- are the ionized impurity concentrations, U_n and U_p are the net electron and hole recombination rates, and J_n and J_p are the carrier current densities expressed by the drift-diffusion model in the form of

$$J_{n,p} = -q\mu_{n,p} n \nabla\varphi_{n,p} \tag{4}$$

where φ_n and φ_p, are the quasi-Fermi levels, and μ_n and μ_p are the carrier mobilities.

The charge Q_t is expressed in terms of the trap concentration N_t, the carrier thermal velocities v_n and v_p, the capture cross sections σ_n, and σ_p, and the emission rates e_n and e_p by using

$$Q_t = qN_t\left[\frac{v_p\sigma_p + e_n}{v_p(\sigma_p+\sigma_n)+(e_n+e_p)} - \frac{v_n\sigma_n + e_p}{v_n(\sigma_p+\sigma_n)+(e_n+e_p)}\right] \tag{5}$$

where $v_n = 1.9\times10^5$ m/s and $v_p = 1.2\times10^5$ m/s at $T = 300$ K [20], and e_n and e_p are calculated as a function of the difference E_{trap} between the trap energy level and the intrinsic Fermi level

$$e_n = v_n\sigma_n n_i \exp\left(\frac{E_{trap}}{kT}\right) \tag{6}$$

$$e_p = v_p\sigma_p n_i \exp\left(-\frac{E_{trap}}{kT}\right). \tag{7}$$

In this analysis, the others key physical models include the Shockley Read Hall (SRH) and Auger recombination processes, the incomplete ionization of dopants and the carrier mobility effects.

The SRH and Auger recombination rates are modeled using the standard expressions [21]

$$R_{SRH} = \frac{pn - n_i^2}{\tau_p\left(n + n_i\exp\left(\frac{E_{trap}}{kT}\right)\right) + \tau_n\left(p + n_i\exp\left(-\frac{E_{trap}}{kT}\right)\right)} \tag{8}$$

$$R_{Auger} = (C_p p + C_n n)(np - n_i^2) \tag{9}$$

where $C_n = 5\times10^{-31}$ cm^6/s and $C_p = 2\times10^{-31}$ cm^6/s are the Auger coefficients [22] and τ_n and τ_p are the carrier lifetimes governed in turn by traps [20] and doping concentration [23]:

$$\tau_{n,p} = \frac{1}{v_{n,p}\sigma_{n,p}N_t} \tag{10}$$

$$\tau_{n,p} = \frac{\tau_{0n,p}}{1+\left(\frac{N}{N_{n,p}^{SRH}}\right)}. \tag{11}$$

Here, N is the total impurity concentration for a given device region and $\tau_{0n} = 500$ ns, $\tau_{0p} = 100$ ns, and $N_{n,p}^{SRH} = 1\times10^{30}$ cm^{-3} are reference parameters taken from [24].

The incomplete ionization of impurities is expressed assuming the Fermi-Dirac statistics by means of [25]

$$N_{A,D}^{-,+} = N_{A,D}\left(\frac{-1+\sqrt{1+4g_{v,c}\frac{N_{A,D}}{N_{V,C}(T)}e^{\frac{\Delta E_{a,d}}{kT}}}}{2g_{v,c}\frac{N_{A,D}}{N_{V,C}(T)}e^{\frac{\Delta E_{a,d}}{kT}}}\right) \tag{12}$$

where N_A and N_D are the substitutional p-type and n-type doping concentrations, N_V and N_C are the hole and electron density of states varying with temperature, g_v = 4 and g_c = 2 are the degeneracy factors of the valence and conduction band and ΔE_a and ΔE_d are the acceptor and donor energy levels, respectively. Considering the nature of the doping species (i.e. Al and N), the ionization energy levels ΔE_a = 190 meV and ΔE_d = 70 meV are assumed [26], [27].

Finally, the carrier mobility is modelled by the Caughey-Thomas equation at T = 300 K, validated for 4H-SiC in [28]:

$$\mu_{n,p} = \mu_{0n,p}^{\min} + \frac{\mu_{0n,p}^{\max} - \mu_{0n,p}^{\min}}{1 + \left(\frac{N}{N_{n,p}^{crit}} \right)^{\delta_{n,p}}} \tag{13}$$

where N is the local concentration of the ionized impurities; $\mu_{0n}^{\min}$ = 40 cm^2/V×s, $\mu_{0p}^{\min}$ = 15.9 cm^2/V×s, $\mu_{0n}^{\max}$ = 950 cm^2/V×s and $\mu_{0p}^{\max}$ = 125 cm^2/V×s are fundamental model parameters taken from [28], [29].

This simulation setup is supported by experimental results on almost similar p-i-n diodes [17], [18], [30], and further parameter details are provided in other recent manuscripts of ours [31]-[34].

IV. Experimental and Modelling

Several 4H-SiC p-i-n diodes (nominally identical) placed on different dies were characterized at room temperature by using a HP4155 Semiconductor Parameter Analyzer. Forward current-voltage measurements allowed to classify most of the devices as well-behaved diodes with good rectifying characteristics. About the 20% of the samples, however, showed distorted I_F-V_F curves with an excess of current under low-voltage test conditions (V_F < 1.9 V) as shown in Fig. 2.

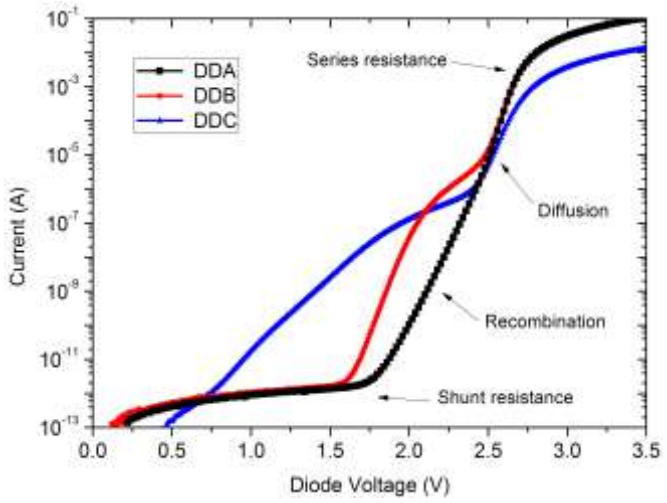

Fig. 2. Experimental I_F-V_F curves of different 4H-SiC p-i-n diodes. A compliance current of 100 mA was imposed during the measurements. The device area is 1×10^{-3} cm^2 for all the samples.

Here, the leaky diode behaviors DDB and DDC can be compared with the typical good quality curve DDA, which is characterized by a sharp turn-on for a forward bias close to 1.9 V and a quick rise in slope. The calculated device area is 1×10^{-3} cm^2 for all the samples since they are characterized by a diameter close to 350 µm.

The diode behaviors DDB and DDC are related to an inhomogeneous epitaxial layer containing intrinsic defects that, regardless of the diode fabrication process give origin to a leakage path or a shunt resistance connected in parallel with the actual p-i-n structure [35]. In other words, depending on the crystal quality of the starting 4H-SiC substrate, the leaky diode current behaviors can be modelled as due to two diodes with different barrier heights connected in parallel, each contributing to the current independently, where the defective device has a lower turn-on voltage. Finally, in Fig. 2 all the samples exhibit a series resistance effect at voltages higher than 2.7 V and the curves tend to become flat. As well known, the series resistance is the sum of the contact contributions and the diode internal resistance.

In order to extract the fundamental device electrical parameters listed in Table I, in the voltage range where the shunt resistance R_{sh} and the series resistance R_s are negligible, we assumed a diode current-voltage conduction model in the form of [36]-[38]

$$I_{tot} = I_{Sdiff}\left[\exp\left(\frac{qV}{n_1 kT}\right) - 1\right] + I_{Srec}\left[\exp\left(\frac{qV}{n_2 kT}\right) - 1\right] \tag{14}$$

where Is_{diff} is the saturation current for diffusion, Is_{rec} is the saturation current for recombination. By taking the natural logarithm of both sides in (14), separately in the voltage range where each of the two exponential term is dominant, we obtained an expression in the form of a linear equation from which we got the slope and, by fitting the experimental results we extracted the diode ideality factors n_1 and n_2. Finally, the R_{sh} and R_s values were extracted from the linear plot of the I_F-V_F curves in Fig. 2. The former at the lower voltage levels and the latter in the voltage range from 2.7 to 2.86 V, namely where the down-bending starts, by calculating the inverse slope of the best linear fit. The linear fit useful for the R_s extraction is shown in Fig. 3.

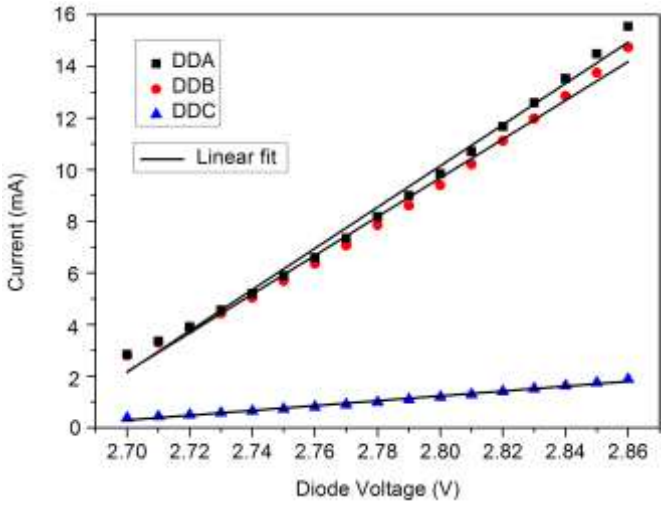

Fig. 3. Linear fit of the I_F-V_F experimental curves in Fig. 2 for the R_s extraction.

By considering the device area (1×10^{-3} cm^2), R_s is in the order of 10 mΩ×cm^2 except for the leaky diode DDC for which we can calculate a value about 10 times higher. In this case, since the contact resistances are identical for all the samples, it is evident that the R_s contribution related to the diode internal resistance is much higher than the other devices.

TABLE I
DIODE ELECTRICAL PARAMETERS

	DDA	DDB	DDC
n_1 @ 2.4 < V_F < 2.7 V	1.35	1.72	2.03
n_2 @ 1.8 < V_F ≤ 2.4 V	2.13	3.38	3.53
R_{sh} (Ω×cm^2)	752×10^6	700×10^6	672
R_s (mΩ×cm^2)	9.4	10.5	106

In the diffusion regime 2.5 < V_F < 2.7 V, the ideality factor n_1 can be considered in the proper value only for the diode DDA (n_1 = 1 for ideal diffusion) whereas the defect effects determine, in particular for the diode DDC, n_1 close to 2. Also, in the low injection regime V_F ≤ 2.5 V, the diodes DDC and DDB have a higher value of n_2 as a consequence of a higher current contribution due to the recombination phenomena.

V. RESULTS AND DISCUSSION

In this section, the impact of trapping effects on the I_F-V_F characteristics presented above is investigated by means of a numerical simulation study. During the simulations, we considered the presence of crystal defects inside the device structure both as a result of the growth of the epitaxial layer and as interactions with energetic particles (Al^+ ions) during the implantation process.

More in detail, the post-annealing residual crystal damage was accounted for in the form of a depth profile of electrically active defects located within the anode region in accordance with the Al doping profile in Fig. 1. Three different profiles were calculated as a fraction of the Al concentration, i.e. 5%, 10%, and 15%, at each depth. From the literature, in fact, we can consider only a percentage around the 90% of the Al implanted atoms to really occupy a substitutional position in the crystal for high doping densities [16], [27], [39]. The relative trap energy level was assumed 0.2 eV from the valence band edge likewise the Al acceptor energy level in 4H-SiC [26], [27]. These traps manifest a donor-like effect. In other words, they are positively charged when empty and capture electrons similarly to ionized donor impurities.

Concerning the material intrinsic defect states, according to literature data supported by deep-level transient spectroscopy (DLTS) measurements, the mostly two deep native defects recognized in the 4H-SiC-based devices are the $Z_{1/2}$ and $EH_{6/7}$ centers [16]. They have the same microscopic origin, namely the carbon vacancy, and are assumed located at 0.6-0.7 eV and 1.6-1.7 eV from the conduction band edge [40]-[42], respectively. The $Z_{1/2}$ traps produce an acceptor-like effect, i.e. they are negatively charged when filled and became neutral when empty. On the other hand, since the bandgap is close to 3.26 eV at room temperature, the $EH_{6/7}$ energy level is a midgap level and the nature of these traps could be uncertain. Most researchers, however, have identified in the n-type 4H-SiC the $EH_{6/7}$ centers as the donor level of a carbon vacancy [40]-[43]. Moreover, the $Z_{1/2}$ and $EH_{6/7}$ concentration ratio should be considered in the order of one [41]-[44].

The defect parameters assumed during the simulations are summarized in Table II. The traps due to the Al implanted profile were labelled as D_{imp} and modelled as in [45] and references therein. Their N_t value refers to the peak concentration calculated from the Al SIMS profile in Fig. 1 assuming a percentage of 5%, 10%, and 15%, respectively. As entry data for modeling, the case 10% was used in all the simulations by default.

TABLE II
DEFECT PARAMETERS

	E_t (eV)	N_t (cm^{-3})	σ_n (cm^2)	σ_p (cm^2)
D_{imp}	0.2	3×10^{18}, 6×10^{18}, 9×10^{18}	2.58×10^{-13}	2.58×10^{-13}
$Z_{1/2}$	0.67	3×10^{13} - 3×10^{16}	2.0×10^{-14}	3.5×10^{-14}
$EH_{6/7}$	1.65	3×10^{13} - 3×10^{16}	2.4×10^{-14}	1.0×10^{-14}

As can be seen, in order to investigate the impact of the native substrate on the diode electrical characteristics, for the intrinsic defects a wide range of N_t was considered starting from a value that we can assume proper for thin 4H-SiC n$^-$-epilayers [10]. The $Z_{1/2}$ and $EH_{6/7}$ locations in the bandgap and capture cross sections are consistent with the literature data [10], [11], [40]-[42].

In a first set of simulations, the relative weight of the $Z_{1/2}$ and $EH_{6/7}$ centers on the diode current behavior was evaluated increasing in turn the N_t value as shown in Figs. 4 and 5, respectively. Here, the experimental curves are also reported for comparison.

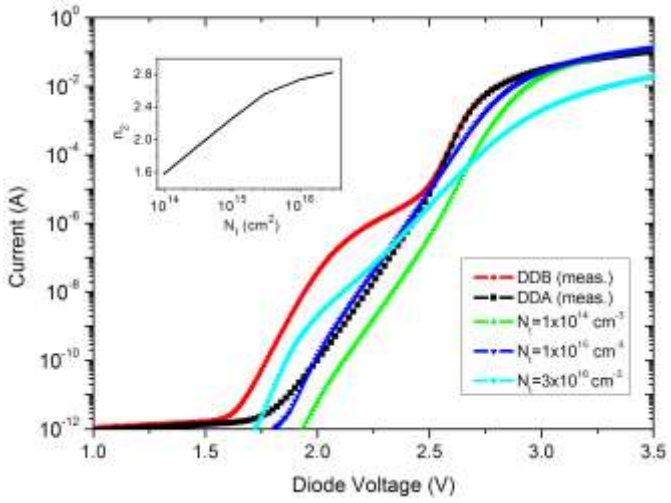

Fig. 4. Measured and simulated I_F-V_F curves for different $Z_{1/2}$ concentrations. The effect of N_t on the ideality factor n_2 is shown in the inset. The $EH_{6/7}$ concentration is fixed to 3×10^{13} cm^{-3}.

From Fig. 4, the $Z_{1/2}$ concentration plays a key role in determining the I_F curve at low and medium forward biases, namely where the recombination and diffusion currents are the dominant components. For a value $N_t = 1\times10^{15}$ cm^{-3} the calculated ideality factor n_2 (see inset) is close to 2.2 in good agreement with the experimental result for the diode DDA in

Table I. On the other hand, a $Z_{1/2}$ concentration exceeding the epilayer doping (i.e., $N_t > 3\times10^{15}$ cm^{-3}) more and more increases the shunt resistance effect and the current behavior tends to the DDB curve. The diode series resistance increases meaningfully for $N_t = 3\times10^{16}$ cm^{-3} and its value becomes comparable with that extracted for the leaky diode DDC ($R_s \approx 100$ mΩ×cm^2).

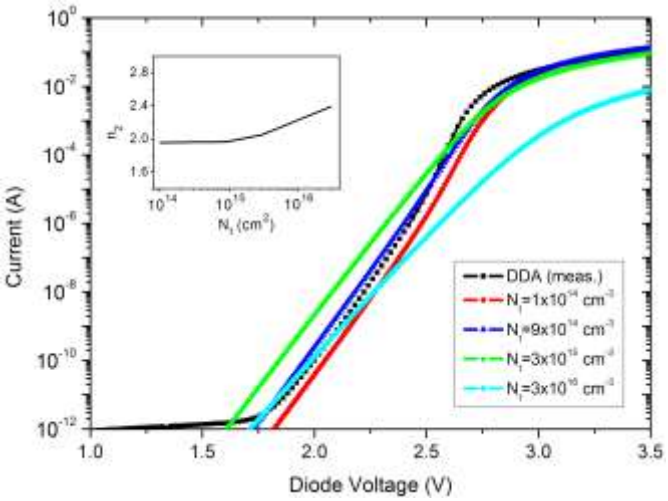

Fig. 5. Measured and simulated I_F-V_F characteristics for different $EH_{6/7}$ concentrations. The effect of N_t on the ideality factor n_2 is shown in the inset. The $Z_{1/2}$ concentration is fixed to 9×10^{13} cm^{-3}.

From Fig. 5, increasing the $EH_{6/7}$ concentration up to a value that approaches the epilayer doping, the curves tend to shift toward lower voltages and up with a moderate change in slope for $V_F \leq 2.5$ V. Then, higher values of N_t have a detrimental effect on R_s that once again tends to the DDC behavior for $N_t = 3\times10^{16}$ cm^{-3}.

The previous analysis was used to achieve the best fit of the DDA curve by considering a combined model of the $Z_{1/2}$ and $EH_{6/7}$ centers with a concentration ratio in the order of one. By tuning the model parameters, the impact of different trap concentrations inside the anode region was also considered. After several attempts, the obtained result is shown in Fig. 6. Here, in particular, the D_{imp} profile was calculated as 5 % of the Al implanted impurities and the intrinsic defect concentrations were tuned to 2.5×10^{14} cm^{-3} and 1.5×10^{14} cm^{-3} for the $Z_{1/2}$ and $EH_{6/7}$ centers, respectively. Finally, in order to fit the curve at the lower voltages ($V_F \leq 1.8$ V), a shunt resistance correspondent to the value extracted for the diode DDA in Table I was imposed for the anode current calculation of the simulated device.

It is worthwhile noting that, fixed the role of the intrinsic defects, an appropriate trap concentration in the anode region improves the fit of the experimental curve at highest current regimes. The simulated I_F -V_F curves for the different D_{imp} profiles considered in this work are shown in Fig. 7. These current behaviors are mainly related to the effective trap concentration inside the implanted region that affects the carrier mobility determining de-facto the diode internal resistance R_i, resulting R_i α $1/qN\mu_n$. At the same time, the carrier trap effects due to the non-substitutional Al doping concentration have almost no impact where the total diode current is governed by the effective carrier lifetime in the drift region.

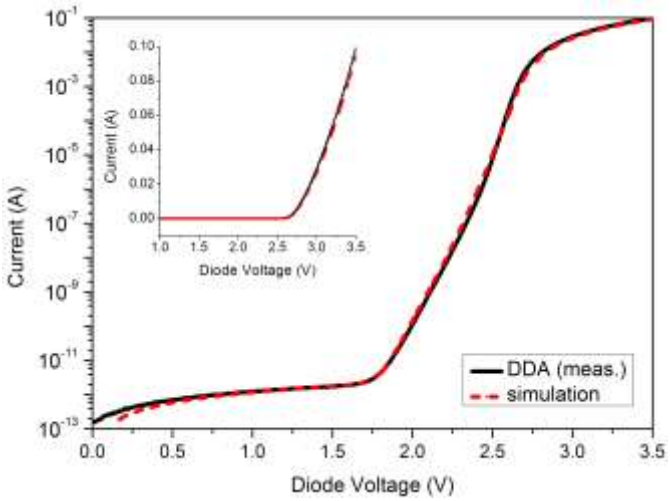

Fig. 6. Measured and simulated I_F-V_F curve for the diode DDA.

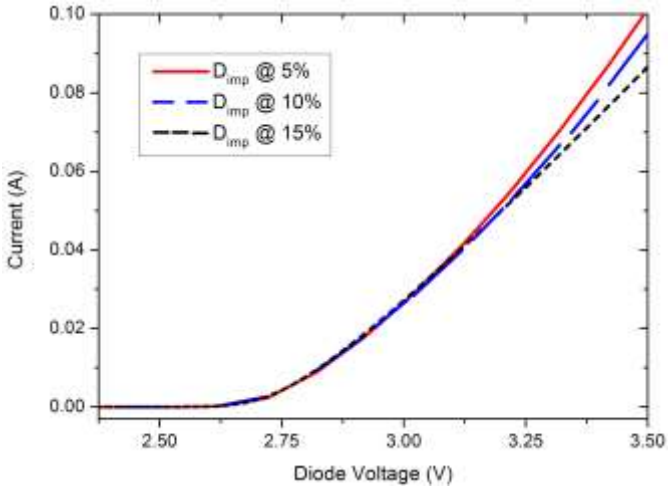

Fig. 7. Impact of different trap concentration profiles in the anode region calculated as a fraction of the Al implanted impurities.

In order to extract interesting information on the device physics, we highlighted the role of the carrier injection into the p-i-n structure by plotting in Fig. 8, for the simulated curve in Fig. 6, the electron and hole concentration profiles as a function of the distance from the anode contact for three different bias voltages. The plot was traced by taking a vertical cut along the diode axis of symmetry.

Due to the defect state concentration that limits the carrier lifetimes (10), a significant carrier injection into the drift region does not start up to V_F is close to 2.7 V. Then, around $V_F = 3$ V the diode reaches the high injection regime and the i-region appears filled of the electron-hole plasma which is required for reaching therein a conductivity modulation regime. The down-bending of the I_F curve in Fig. 6 is therefore related to a significant minority carrier injection into the diode terminal regions where the carriers recombine.

The corresponding carrier recombination depth profiles are shown in Fig. 9.

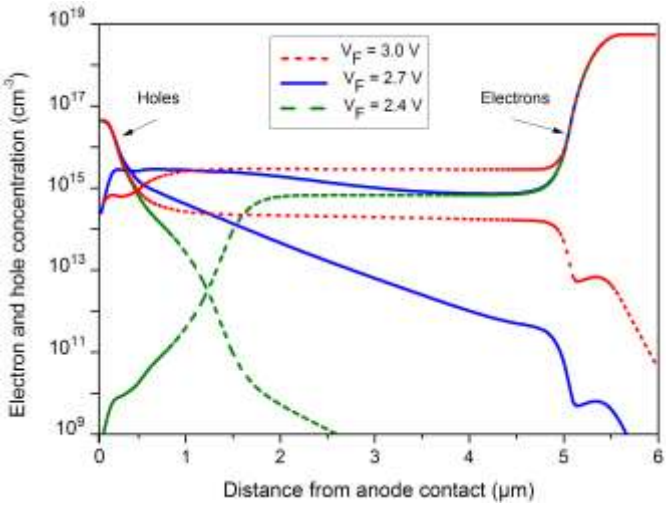

Fig. 8. Electron and hole concentration profiles at different forward biases. The drift region doping concentration is 3×10^{15} cm^{-3}.

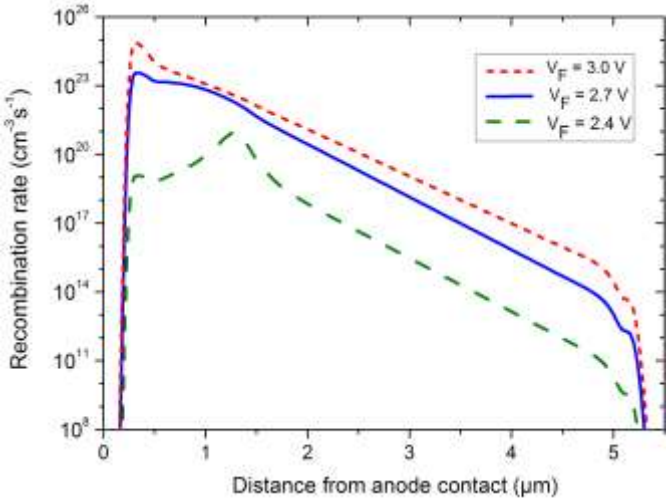

Fig. 9. Carrier recombination depth profiles at different forward biases.

As expected, up to V_F = 2.4 V the dominant component of I_F is the recombination current which originates in the drift region supported by the trap-assisted recombination phenomena. Then, the increased recombination rates tend to be concentrated more and more in the anode region. Above the curve knee ($V_F \geq 2.7$ V), in fact, the diode current is largely dominated by the electron injection into the anode, being the concentration of free holes for conduction strongly limited in turn by the incomplete activation of the ion implanted impurities and the trap activity. On one hand, the incomplete ionization model (12) predicts a saturation level of the ionized acceptor concentration in the anode over 10 times lower with respect to that of donors in the n^+-region. On the other hand, the large cross sections σ_p of the intrinsic defects, in particular of the $Z_{1/2}$ centers, capture the holes injected from the anode very effectively.

Simulation results for different values of the capture cross sections in the same decade as proposed in [11], and preserving the σ_p/σ_n ratio, showed a limited impact on the diode current capabilities confirming the presented analysis.

VI. Conclusion

In this work, the impact of recombination and trapping effects on the measured forward I_F-V_F curves of Al implanted 4H-SiC p-i-n diodes has been investigated by means of a fine-tuned numerical model. The combined activity of both intrinsic and doping-induced deep-defects were considered during the simulations. The experimental devices were classified as well-behaved and leaky diodes. Their fundamental electrical parameter were extracted and used for comparison.

$Z_{1/2}$ and $EH_{6/7}$ centers in the device active region reduce the effective carrier lifetimes and increase the local recombination rate varying the ideality factor from its reference value that is slightly above 2 in the recombination region and in the order of 1.3 in the diffusion regime. In addition, a concentration of intrinsic defects that becomes comparable to the epilayer doping has a strongly effect on the shunting phenomena at lower voltages and at the same time increases the diode series resistance over 10 times at high current levels. A detrimental effect on the series resistance is also observed accounting for an explicit trap concentration confined in the anode region due to the post-annealing residual crystal damage created by the Al^+ ion implantation process. These traps increase the diode internal resistance introducing high-resistive paths.

Acknowledgment

The authors would like to thank R. Nipoti and the staff of the institute for Microelectronics and systems (CNR-IMM, Bologna, Italy) for supplying the 4H-SiC diodes.

References

[1] R. Wang, D. Boroyevich, P. Ning, Z. Wang, F. Wang, P. Mattavelli, K. Ngo, and K. Rajashekara, "A high-temperature SiC three-phase AC-DC converter design for >100°C ambient temperature," *IEEE Trans. Power Electron.*, vol. 28, no. 1, pp. 555-572, 2013. DOI: 10.1109/TPEL.2012.2199131.

[2] G. Calderon-Lopez, A. J. Forsyth, D. L. Gordon, and J. R. McIntosh, "Evaluation of SiC BJTs for high-power DC-DC converters," *IEEE Trans. Power Electron.*, vol. 29, pp. 2474-2481, 2014. DOI: 10.1109/TPEL.2013.2273293.

[3] M. C. Lee, and A. Q. Huang, "An injection efficiency model to characterize the injection capability and turn-off speed for >10 kV 4H-SiC IGBTs," *Solid-State Electron.*, vol. 93, pp. 27-39, 2014. DOI: 10.1016/j.sse.2013.12.008.

[4] L. Lin, J. H. Zhao, "Simulation and experimental study of 3-step junction termination extension for high-voltage 4H-SiC gate turn-off thyristors," *Solid-State Electron.*, vol. 86, pp. 36-40, 2013. DOI: 10.1016/j.sse.2013.04.029.

[5] B. J. Baliga, *Silicon Carbide Power Devices*, World Scientific, Singapore, 2005.

[6] K. Kawahara, M. Krieger, J. Suda, and T. Kimoto, "Deep level induced by reactive ion etching in n- and p-type 4H-SiC," *J. Appl. Phys.*, vol. 108, p. 023706, 2010. DOI: 10.1063/1.3460636.

[7] K. Kawahara, G. Alfieri, and T. Kimoto, "Detection and depth analyses of deep levels generated by ion implantation in n- and p-type 4H-SiC," *J. Appl. Phys.*, vol. 106, p. 013719, 2009. DOI: 10.1063/1.3159901.

[8] M. Usman, M. Nawaz, and A. Hallén, "Position dependent bulk traps and carrier compensation in 4H-SiC bipolar junction transistors," *IEEE*

Trans. Electron Devices, vol. 278, pp. 258–265, 2013. DOI: 10.1109/TED.2012.2226586.

[9] L. Storasta, J. P. Bergman, C. Hallin, and E. Jenzen "Electrical activity of residual boron in silicon carbide," *Mater. Science Forum*, vol. 389-393, pp. 549-552, 2002. DOI: 10.4028/www.scientific.net/MSF.389-393.549.

[10] P. B. Klein, and B. V. Shanabrook, "Lifetime-limiting defects in n- 4H-SiC epilayers," *J. Appl. Physics*, vol. 88, p. 052110, 2006. DOI: 10.1063/1.2170144.

[11] P. B. Klein, "Carrier lifetime measurements in n- 4H-SiC epilayers," *J. Appl. Phys.*, vol. 103, p. 033702, 2008. DOI: 10.1063/1.2837105.

[12] F. Zhao, M. M. Islam, B. K. Daas, and T. S. Sudarshan, "Effect of crystallographic dislocations on the reverse performance of 4H-SiC p-n diodes," *Materials letters*, vol. 64, pp. 281-283, 2010. DOI: 10.1016/j.matlet.2009.10.062.

[13] J. B. Fedison, N. Ramungul, T. P. Chow, M. Ghezzo, and J. W. Kretchmer, "Electrical characteristics of 4.5kV implanted anode 4H-SiC PiN junction rectifiers," *IEEE Electron Dev. Lett.*, vol. 22, pp. 130-132, 2001. DOI: 10.1109/55.910619.

[14] M. L. Megherbi, F. Pezzimenti, L. Dehimi, A. Saadoune, and F. G. Della Corte, "Analysis of the forward I-V characteristics of Al-implanted 4H-SiC p-i-n diodes with modeling of recombination and trapping effects due to intrinsic and doping-induced defect states," *J. Electron. Mater.*, vol. 47, pp.1414-1420, 2018. DOI: 10.1007/s11664-017-5916-8.

[15] R. Nipoti, F. Moscatelli, P. De Nicola, "Al+ implanted 4H-SiC p+-i-n diodes: forward current negative temperature coefficient", *IEEE Electron Dev. Lett.,* vol. 34(8), pp. 966–8, 2013. DOI: 10.1109/LED.2013.2269863.

[16] Z. C. Feng, and J. H. Zhao, *Silicon Carbide: Materials, Processing and Devices*, Taylor & Francis, New York, 2004, chs. 6, 5, 4.

[17] M. L. Megherbi, F. Pezzimenti, L. Dehimi, S. Rao, and F. G. Della Corte, "Analysis of different forward current-voltage behaviours of Al implanted 4H-SiC vertical P-i-N diodes," *Solid-State Electron*., vol. 109, pp. 12-16, 2015. DOI: 10.1016/j.sse.2015.03.001.

[18] F. Pezzimenti, F. G. Della Corte, R. Nipoti, "Experimental characterization and numerical analysis of the 4H-SiC p–i–n diodes static and transient behavior," *Microelectronics Journal*, vol. 39, pp.1594-1599, 2008. DOI: 10.1016/j.mejo.2008.02.005.

[19] Yu. Goldberg, M. E. Levinshtein, and S. L. Rumyantsev, *Properties of Advanced Semiconductor Materials GaN, AlN, InN, BN, SiC, SiGe,* J. Wiley & Sons, New York, 2001, ch. 5.

[20] Silvaco Atlas User's Manual, Device Simulator Software, 2013.

[21] S. Selberherr, *Analysis and Simulation of Semiconductor Devices*, Springer, Wien, 1984.

[22] A. Galeckas, J. Linnros, V. Grivickas, U. Lindefelf, C. Hallin, "Auger recombination in 4H-SiC: Unusual temperature behaviour," *Appl. Phys. Lett.*, vol. 7, pp. 1:3269-71, 1997. DOI: 10.1063/1.120309.

[23] P. T. Landsberg, and G. S. Kousik, "The connection between carrier lifetime and doping density in nondegenerate semiconductors," *J. Appl. Physics*, vol. 56, pp. 1696-1700, 1984. DOI: 10.1063/1.334159.

[24] M. Bakowski, U. Gustafsson and U. Lindefelt, "Simulation of SiC high power devices," *Physica Status Solidi A*, vol. A 162, pp. 421-429, 1997. DOI: 10.1002/1521-396X(199707)162:1<421::AID-PSSA421>3.0.CO;2-B.

[25] M. Ruff, H. Mitlehner and R. Helbig, "SiC Devices Physics and Numerical Simulation," *IEEE Trans. Electron Devices*, vol. 41, pp.1040-1054, 1994. DOI: 10.1109/16.293319.

[26] T. Ayalew, T. Grasse, H. Kosina, S. Selberherr, "Modeling of lattice site-dependent incomplete ionization in a-SiC devices," *Material Science Forum,* vol. 483, pp. 845–8, 2005. DOI: 10.4028/www.scientific.net/MSF.483-485.845.

[27] T. Troffer, M. Schadt, T. Frank, H. Itoh, G. Pensl, J.Heindl, H. P. Strunk, and M. Maier, "Doping of SiC by Implantation of Boron and Aluminium," *Physica status solidi*, vol. 162, pp. 277-298, 1997. DOI: 10.1002/1521-396X(199707)162:1<277::AID-PSSA277>3.0.CO;2-C.

[28] M. Roschke, and F. Schwierz, "Electron Mobility Models for 4H, 6H, and 3C SiC", *IEEE Trans. Electr. Dev*., vol. 48, pp. 1442-1447, 2001. DOI: 10.1109/16.930664.

[29] X. Li, Y. Luo, L. Fursin, J. H. Zhao, M. Pan, P. Alexandrov, M. Weiner, "On temperature coefficient of 4H-SiC BJT current gain," *Solid-State Electronics*, vol.47, pp.233-239, 2003. DOI: 10.1016/S0038-1101(02)00200-9.

[30] F. Pezzimenti, L. F. Albanese, S. Bellone, and F. G. Della Corte, "Analytical model for the forward current of Al implanted 4H-SiC p-i-n diodes in a wide range of temperatures," in Proc. IEEE Int. Conf. *Bipolar/BiCMOS Circuits and Technology Meeting*, 2009, pp. 214-217. DOI: 10.1109/BIPOL.2009.5314147.

[31] F. Pezzimenti, "Modeling of the steady state and switching characteristics of a normally-off 4H-SiC trench bipolar-mode FET" *IEEE Trans Electron Devices*, vol. 60, pp. 1404-1411, 2013. DOI: 10.1109/TED.2013.2244603.

[32] G. De Martino, F. Pezzimenti, F. G. Della Corte, G. Adinolfi, and G. Graditi, "Design and numerical characterization of a low voltage power MOSFET in 4H-SiC for photovoltaic applications", In Proc. IEEE Int. Conf. *Ph. D. Research in Microelectronics and Electronics - PRIME,* 2017, pp. 221-224. DOI: 10.1109/PRIME.2017.7974147.

[33] F. G. Della Corte, F. Pezzimenti, S. Bellone, and R. Nipoti, "Numerical simulations of a 4H-SiC BMFET power transistor with normally-off characteristics," *Mater. Science Forum*, vol. 679-680, pp. 621-624, 2011. DOI: 10.4028/www.scientific.net/MSF.679-680.621.

[34] F. Pezzimenti, and F. G. Della Corte, "Design and modeling of a novel 4H-SiC normally-off BMFET transistor for power applications", in Proc. *Mediterranean Electrotechnical Conference - MELECON*, 2010, pp. 1129-1134. DOI: 10.1109/MELCON.2010.5476362.

[35] T. Dalibor, G. Pensl, H. Matsunami, T. Kimoto, W. J. choyke, A Schoner, and N. Nordell, "Deep defect centers in silicon carbide monitored with deep level transient spectroscopy," *Phys. Stat. Sol. (a),* vol. 162, pp.199-225, 1997. DOI: 10.1002/1521-396X(199707)162:1<199::AID-PSSA199>3.0.CO;2-0.

[36] D. Peters, R. Schorner, K. H. Holzlein, and P Friedrichs, "Planar aluminum-implanted 1400 V 4 H silicon carbide p-n-diodes with low on resistance," *Appl. Phys. Lett.*, vol. 71, pp. 2996-2997, 1997. DOI: 10.1063/1.120241.

[37] M. Wolf, G. T. Noel, and R. J. Stirn, "Investigation of the double exponential in the current-voltage characteristics of silicon solar cells," *IEEE Trans. Electron Devices*, vol. 24, pp. 419-428, 1977. DOI: 10.1109/T-ED.1977.18750.

[38] S. Banerjee, and W. A. Anderson, "Conduction Mechanisms in Radiation Damaged MINP Si Solar Cells," *IEEE Trans. Nucl. Science*, vol. 33, pp. 1474-1481, 1986. DOI: 10.1109/TNS.1986.4334626.

[39] M. V. Rao, J. B. Tucker, M. C. Ridgway, O. W. Holland, N. Papanicolaou, and J. Mittereder, "Ion implantation in bulk semi-insulating 4H-SiC," *J. Appl. Physics*, vol. 86(2), pp. 752-758, 1999. DOI: 10.1063/1.370799.

[40] W. C. Mitchel, and W. D. Mitchell, "Compensation mechanism in high purity semi-insulating 4H-SiC," *J. Appl. Physics*, vol. 101, p. 053716, 2007. DOI: 10.1063/1.2437677.

[41] T. Hornos, A. Gali, and B. G. Svensson, "Large-scale electronic structure calculations of vacancies in 4H-SiC using the Heyd-Scuseria-Ernzerhof screened hybrid density functional," *Mater. Science Forum*, vol. 679-680, pp. 261-264, 2011. DOI: 10.4028/www.scientific.net/MSF.679-680.261.

[42] N. T. Son, X. T. Trinh, L. S. Løvlie, B. G. Svensson, K. Kawahara, J. Suda, T. Kimoto, T. Umeda, J. Isoya, T. Makino, T. Ohshima, and E. Janzén, "Negative-U system of carbon vacancy in 4H-SiC," *Phys. Rev. Lett.*, vol. 109, p. 187603, 2012. DOI: 10.1103/PhysRevLett.109.187603.

[43] B. Zippelius, A. Glas, H. B. weber, G. Pensl, T. Kimoto, and M. Krieger "$Z_{1/2}$- and EH_6-center in 4H-SiC: not identical defects?," *Mater. Science Forum*, vol. 717-720, pp. 251-254, 2014. DOI: 10.4028/www.scientific.net/MSF.717-720.251.

[44] K. Danno, and T. Kimoto, "Investigation of deep levels in n-type 4H-SiC epilayers irradiated with low-energy electrons," *J. Appl. Physics*, vol. 100, p. 113728, 2006. DOI: 10.1063/1.2401658.

[45] F. Pezzimenti, F. G. Della Corte, and R. Nipoti, "Numerical simulations of Al implanted 4H-SiC diodes modeling an explicit carrier trap effect due to the non-substitutional Al doping concentration," in *Proc. IEEE BCTM*, pp. 214–217, 2009. DOI: 10.1109/BIPOL.2009.5314142.

M. Larbi Megherbi received the B.Sc. degree in electronic engineering from Batna University, the M.Sc. degree in magnetic material from University of Wales, Cardiff, and the Ph.D. degree in electrical engineering from Biskra University in 1986, 1988, and 2015, respectively.

His research area include simulation of power semiconductor devices with focus on PiN diodes. His other interests include simulation of wide bandgap devices and radiation detector. He is currently with the LMSM laboratory for semiconductor material, Biskra, Algeria.

Fortunato Pezzimenti received the Laurea degree in electronic engineering from Mediterranea University of Reggio Calabria, Italy, in 2000 and the Ph.D degree in 2004. Since 2006, he is Assistant Professor of Electronics at the Mediterranea University of Reggio Calabria.

His current research interests include design, modeling, and electrical characterization of wide bandgap semiconductor devices for high power, high frequency, and high temperature applications. He also works on multi-junction solar cells.

Lakhdar Dehimi received the D.E.S degree (Diploma of higher Education) in Electronic Physics from Batna University in 1985, the M.Sc. degree in magnetic material from the University of Wales in 1988, and the Ph.D. degree in Microelectronics from Batna University in collaboration with School of Physics Lancaster University in 2004. He obtained the grade of Professor in Physics in 2009.

His research area include modeling and simulation of semiconductors devices. His main topic is study of traps effects on the electrical characteristics. Also, he carried out research on multi-junction solar cell. He is currently senior lecturer at the Physics Department of Batna University and Head of Group at the LMSM Laboratory Biskra University, Algeria.

M. Achour Saadoune received the Ing. degree in electronics, the M.Sc. degree in electronics, the Ph.D. degree in electrical engineering, and the HDR. degree in electrical engineering all from Biskra University, Algeria, in 2001, 2004, 2009, and 2014, respectively.

He is currently a researcher at the Laboratory of Metallic and Semiconducting Materials (LMSM), University of Biskra, Algeria. His research interests include simulation of power semiconductor devices, solar cells (multiple quantum well, multi-junction and nanostructures) and effects of radiation damage on semiconductor.

Francesco G. Della Corte (M'98) received the Laurea degree in electronic engineering from the University of Napoli, Naples, Italy, in 1988.

He is currently a Full Professor of Electronics with the Mediterranea University of Reggio Calabria, Reggio Calabria, Italy.

His research topics include wide bandgap semiconductor device modeling for high temperature and high power applications, silicon photonics and wireless smart sensors.

DOI: 10.1109/TED.2018.2849693